Ultrasound in Med. & Biol., Vol. ■, No. ■, pp. 1–15, 2010

0301-5629/$ - see front matter

ELSEVIER

doi:10.1016/j.ultrasmedbio.2010.07.004

● *Original Contribution*

QUANTITATIVE ASSESSMENT OF ARTERIAL WALL BIOMECHANICAL PROPERTIES USING SHEAR WAVE IMAGING

MATHIEU COUADE,* MATHIEU PERNOT,† CLAIRE PRADA,† EMMANUEL MESSAS,‡ JOSEPH EMMERICH,‡ PATRICK BRUNEVAL,‡ ALINE CRITON,* MATHIAS FINK,† and MICKAEL TANTER†

*SuperSonic Imagine, Aix en Provence, France; †Institut Langevin, ESPCI-ParisTech, CNRS UMR 7587, Inserm U979, Paris, France; and ‡APHP, Hopital Europeen Georges Pompidou, Paris, France; INSERM U765, Paris, France

(*Received* 18 *February* 2010; *revised* 8 *June* 2010; *in final form* 4 *July* 2010)

Abstract—A new ultrasound-based technique is proposed to assess the arterial stiffness: the radiation force of an ultrasonic beam focused on the arterial wall induces a transient shear wave (∼10 ms) whose propagation is tracked by ultrafast imaging. The large and high-frequency content (100 to 1500 Hz) of the induced wave enables studying the wave dispersion, which is shown experimentally *in vitro* and numerically to be linked to arterial wall stiffness and geometry. The proposed method is applied *in vivo*. By repeating the acquisition up to 10 times per second (theoretical maximal frame rate is ∼100 Hz), it is possible to assess *in vivo* the arterial wall elasticity dynamics: shear modulus of a healthy volunteer carotid wall is shown to vary strongly during the cardiac cycle and measured to be 130 ± 15 kPa in systole and 80 ± 10 kPa in diastole. (E-mail: mathieu.couade@gmail.com) **© 2010 World Federation for Ultrasound in Medicine & Biology.**

Key Words: **Arterial stiffness, Elastography, Ultrasound, Acoustic radiation force, Vascular imaging.**

INTRODUCTION

The mechanical properties of the arteries play a central role in cardiovascular function (O'Rourke et al. 2002). A direct relationship between arterial stiffness and various cardiovascular diseases has been established, making arterial stiffness an important predictor of cardiovascular morbidity and mortality (Cheng et al. 2002). Each type of artery has specific composition and mechanical properties that can evolve differently with pathologies. It is well known for instance that arterial stiffness increases with aging or hypertension, leading to an increased risk of cardiovascular acute events such as stroke and myocardial infarction (Laurent et al. 2001). A softening of arteries can also occur, for instance in many cases of aneurysm. Although the change in viscoelastic properties of arteries is generally systemic and affects the whole vascular system, arteries at different sites respond differently to aging (Boutouyrie et al. 1992), hypertension (van den Berkmortel et al. 2001) or pregnancy, where the carotid artery has been found to stiffen, whereas the aorta becomes softer (Mersich et al. 2005). The viscoelastic properties of arteries have been extensively investigated over the last decades and, recently, serious attention has been directed at more precise measurement of arterial stiffness. Because this challenging issue remains complex *in vivo*, the most complete studies have been performed *ex vivo* on artery samples (Deng et al. 1994). These studies have shown that the elastic properties of the arterial wall are anisotropic, reflecting their structural anisotropy, and nonlinear because they are strongly varying with respect to the intraluminal blood pressure. In other words, because of the large variations of arterial pressure, the arterial stiffness varies during the cardiac cycle.

Different indices have been introduced to quantify the arterial stiffness (Laurent et al. 2006). Most existing techniques for arterial stiffness estimation are based on the analysis of the arterial pulse wave travelling through the artery. This pulse wave has been extensively studied and used for years for prognostics of cardiovascular diseases and to assess and monitor cardiovascular event risks. This physiological wave takes its origin in the systolic peak pressure corresponding to the ejection of blood through the aorta. Because the arterial wall is

Video Clips cited in this article can be found online at: http://www.umbjournal.org.

Address correspondence to: Mathieu Couade, Les jardins de la Duranne - Bât E & F, 510 Rue René Descartes, 13857 Aix-en-Provence, France. E-mail: mathieu.couade@gmail.com

elastic, this local overpressure results in a local increase of the aortic radius. This perturbation propagates along the aorta and then along the arterial tree. Several existing techniques attempt to retrieve information on arterial stiffness from the analysis of properties of this wave, such as its velocity or its shape. For instance, the propagation speed (pulse wave velocity [PWV]) can provide an estimate of the arterial wall Young's modulus. The Moens-Korteweg equation and its extensions are often used to derive the Young's modulus, although these simplified models contain unrealistic assumptions (Ambartsumyan and Movsisyan 1978) such as the assumption of an infinitely long tube isolated in vacuum (external free boundary condition instead of considering the solid-solid boundary condition between the arterial wall and the surrounding tissues) and filled with incompressible nonviscous fluid. Moreover, although the propagation of the pulse wave is strongly nonlinear, the pulse wave is often considered as propagating linearly: in the Moens-Korteweg model, the propagation speed is obtained by linearization of Euler fluid dynamic equations governing the propagation of the wave (Korteweg 1878):

$$c=\sqrt{\frac{Eh}{2R\rho}}. \tag{1}$$

The pulse wave is intrinsically a compressional pressure wave propagating in blood but is affected by boundary properties such as Young's modulus E, radius R, thickness h and density ρ of the arterial wall. A direct estimation of the PWV can be done by measuring the propagation time of the pulse between two arterial sites separated by a known distance using two or more pressure sensors attached to the skin (Asmar et al. 1995). Although this method is robust and gives an average (or global) estimate of the PWV over a part of the arterial tree, the Young's modulus is not accurately estimated because of errors on the distance between the two measurement sites. To obtain a local estimate of the PWV, real-time ultrasound imaging with a reduced number of transmitted beams, known as pulse wave imaging, has been proposed by Kanai et al. (2000) and later studied by other groups (Eriksson et al. 2002; Sorensen et al. 2008). The same principle has been applied in magnetic resonance imaging (Bolster et al. 1998). These approaches consist in measuring the radial displacements caused by the pulse wave propagation. Other studies have also shown that the propagation of the pulse wave can be imaged based on the retrospective electrocardiogram (ECG) gating technique (Pernot et al. 2007) or in a single cardiac cycle using plane-wave imaging (Hasegawa and Kanai 2008; Sorensen et al. 2008) or multiple M-Mode ultrasound (Hermeling et al. 2009). Another method for assessing locally the arterial stiffness relies on quantifying the motion of the arterial wall along the cardiac cycle. Ultrasound echo tracking techniques can provide the arterial stiffness based on the estimation of both the intraluminal pressure (P) and the variation of the arterial cross-sectional area (A) during a complete cardiac cycle (Meinders and Hoeks 2003). The arterial wall distensibility can be estimated by:

$$D=\frac{1}{A}\frac{dA}{dP}. \tag{2}$$

Bramwell and Hill (1922) proposed an analytical relationship between the distensibility and the PWV. The main weakness of this technique is the lack of a noninvasive method to measure locally the blood pressure and the need of estimating the pressure through external sensors, requiring a model (transfer function) to recover an estimation of the actual arterial pressure (Paini et al. 2007; Mahieu et al. 2010). The principle of strain imaging has been also applied to intravascular elastography to assess the local arterial wall strain. This technique has been shown to be very sensitive for plaque characterization (Schaar et al. 2003) but is limited by its invasive nature.

All these techniques assume that viscoelastic properties of the arterial wall are invariant during the cardiac cycle. However, it has been shown that the arterial wall elasticity varies nonlinearly with arterial blood pressure (Fung 1993), meaning that the intrinsic elasticity of the wall changes when the pulse wave distends the artery. Thus, the propagation of the arterial pulse is intrinsically nonlinear because the pulse modifies its local propagation speed. Because the arterial wall does not follow Hooke's law within the range of strain induced by the arterial pressure (typical radial strain ∼10%), all of those previous techniques based on the arterial pulse can only provide at best an average estimate of the arterial wall elasticity over the cardiac cycle. Thus, being able to measure the variation of arterial wall elasticity over a complete cardiac cycle would not only provide a more accurate estimation of arterial stiffness but would also give access to the nonlinear properties of the arterial elastic modulus. Because almost all biological tissues have a nonlinear stress/strain relationship, a complete characterization of tissues' elastic properties is required to measure stiffness over the full physiological range of stress. In the case of artery, the stiffness and nonlinearity with arterial pressure is crucial for the arterial stability itself, as well as for a healthy operation of the whole cardiovascular system (Shadwick 1999). Also, in the presence of plaque, the measurement of arterial stiffness at the different physiological pressure (diastole/systole) could also improve the detection of instable plaque.

To obtain local, instantaneous and quantitative stiffness measurements, one cannot simply rely on the compressional wave generated by the arterial pulse

because this natural wave is available only one time per cycle. To overcome this limitation, another kind of mechanical waves, known as shear waves, can be used for sensing the arterial wall several times per second. For the generation of these mechanical waves, an independent mechanical excitation source is required and can be provided by the acoustic radiation force of a focused ultrasonic beam. The concept of such a remote palpation induced by a focused ultrasonic beam was introduced in the medical imaging community by Sarvazyan et al. (1998). Trahey et al. (2004) have proposed the use of the acoustic radiation force impulse method to remotely push the arterial wall and image the wall relaxation at the pushing location. Although this method provides a mapping of the arterial wall stiffness, it is not quantitative and cannot be used to derive a reference index of arterial stiffness. Zhang et al. have proposed the remote excitation of ring resonance modes (2006) (Zhang and Greenleaf 2006) and bending waves (2005). These waves were imaged by using an optical vibrometry system to detect the small vibrations generated by the acoustic radiation force on the arterial wall.

In this paper, we propose another approach whose "real time" capabilities enable measuring quantitatively the arterial wall stiffness throughout the cardiac cycle several times per cardiac cycle. Our method is based on the generation of a shear wave (typically in the first kHz range) that propagates along the arterial wall. Similarly to the previous techniques, this wave is generated *via* the acoustic radiation force of an ultrasonic beam focused on the arterial wall. However, the originality of our approach consists in measuring the shear wave propagation speed instead of measuring the displacement amplitude within the pushing beam. This is done by acquiring at very high frame rates (up to 10,000 fps) ultrasound images of the transient tissue motions caused by shear wave propagation. This concept, called supersonic shear imaging (SSI), has been introduced by Bercoff et al. (2004). In the field of breast lesion imaging, its interest was recently studied *in vivo* in preliminary clinical investigations by Tanter et al. (2008). Its *in vivo* technical feasibility was also demonstrated for quantitative elasticity imaging of the liver (Muller et al. 2009), muscle (Deffieux et al. 2009) and cornea (Tanter et al. 2009) and the monitoring of ultrasonic thermal ablation (Bercoff et al. 2004). The applicability of the SSI method to image shear wave propagation in the arterial wall and image arterial elasticity is studied. For the recovery of quantitative Young's modulus from Lamb wave propagation speed, the theoretical problem of the complex elastic wave propagation in soft plates and tubes is first studied. A numerical modeling and an analytical solution are derived and validated experimentally on phantoms modeling the arterial wall. Second, although acoustic intensities used in the SSI modality remains below the FDA requirements, a safety study with respect to the generation of the ultrasonic radiation force on the arterial wall is performed on 10 sheep. Finally, the feasibility of the SSI method is shown *in vivo* on the carotid artery: the real time capability of this technique is demonstrated as a method for noninvasive and quantitative measurement of the arterial stiffness that could potentially be performed more than 50 times per second. For this purpose, transient dynamics of the carotid elasticity changes during a single cardiac cycle are acquired.

MATERIAL AND METHODS

Theoretical study of shear wave propagation in arterial wall

Compared with ultrasonic waves, shear waves have very different characteristics in human tissues. Ultrasound is a compressional wave in the MHz range (with a typical millimetric wavelength). When propagating in human soft tissues, these compressional waves encounter an almost homogeneous medium with weak heterogeneities (sound speed is almost constant in soft tissues ranging from 1450 to 1700 m/s). On the contrary, because soft tissues can exhibit very strong contrasts in terms of shear modulus (or stiffness), shear waves can encounter strong reflections or reverberations. Moreover, shear waves can propagate in our soft tissues only at low frequencies (1 to 1000 Hz) because of the important shear viscosity occurring at higher frequency (>kHz), leading to centimetric wavelengths. Hence, in particular configurations (such as arteries), this shear wavelength becomes larger than local strong heterogeneities, leading to guided mode propagation.

The conventional SSI approach such as breast or liver elastography relies on the generation of a large plane shear wave (in the imaging plane), which is considered as propagating in a locally homogeneous medium. When the generated shear wave is traveling in a homogeneous medium, its propagation speed is equal to the bulk shear wave speed (c_T). One can deduce the shear and Young's modulus (μ,E) from the estimation of the shear wave speed (c_T) using the simple formula (Royer and Dieulesaint 2000):

$$\mu = \rho c_T^2, E \approx 3\mu. \quad (3)$$

However, the free space assumption is not correct for shear wave propagation in the arterial wall. The arterial wall is a thin and stiff cylindrical shell (Young's modulus E $\sim$ 300 kPa, wall thickness h $\sim$ 1 mm), embedded in softer soft tissues (E = 30 kPa) and filled with blood, whereas shear waves are evanescent (purely viscous material, dynamic viscosity: $\eta \sim 1e^{-6}$ m^2/s,

frequency f >100 Hz, penetration depth: $\delta << 1$ mm). The thickness of the arterial wall is typically small compared with the shear wavelength (1 to 10 mm). Because of reflections and mode conversions at each interface of the arterial wall with soft tissues and blood, the shear wave propagation is much more complex than in free-space conditions. Those multiple reflections have two effects: (i) Reflections tend to confine the mechanical energy within the wall, which behaves as a wave guide; and (ii) it creates multiple propagation paths for the shear wave. Because two different paths interfere constructively only in certain geometrical conditions (phase matching), each frequency component propagates with a different phase velocity. At the initial time, when the acoustic radiation force is applied, there is no time delay between the frequency components contained in the shear wave packet. Then, as each frequency component propagates at a different speed, the wave packet is dispersed and the shape of the wave packet distorted. Guided waves in elastic plates and tubes have been extensively studied in various cases (isotropic/anisotropic medium, tube, plate, multilayered structures, *etc.*). The theory of guided wave in plate and cylindrical structures has been widely applied to perform nondestructive testing (NDT) of samples based on the generation and the detection of guided wave (Royer and Dieulesaint 2000). Guided waves propagating along a free plate can be separated in two uncoupled kinds of waves: Love waves (the displacements have a zero projection on the normal to the plate) or Lamb waves (the projection of the displacements on the normal to the plate is nonzero). In our experimental setup, the acoustic radiation force is applied orthogonally to the plate, meaning only Lamb waves are generated. There are two kinds of Lamb modes: antisymmetric A_n ($n = 0 \ldots \infty$) and symmetric S_n ($n = 0 \ldots \infty$). Here, we restrict our study to the zero-order Lamb modes in the low-frequency range of shear wave propagation. Indeed, zero-order modes can propagate at any frequency, whereas an n-order symmetric or antisymmetric mode (n>0) has a low frequency cut-off given, respectively, by eqns (4) and (5) (Royer and Dieulesaint 2000), where c_L is the longitudinal bulk velocity, c_T is the shear bulk velocity and h is the thickness of the plate:

$$f_{2n} = \frac{nc_T}{\pi h}, f_{2n+1} = \frac{(n+1/2)c_L}{\pi h}, \tag{4}$$

$$f_{2n} = \frac{nc_L}{\pi h}, f_{2n+1} = \frac{(n+1/2)c_T}{\pi h}. \tag{5}$$

According to typical value of shear and bulk modulus in arteries, $c_L = 1500\ m/s, c_T > 8\ m/s, h < 2\ mm$, cut-off frequencies of these modes are above the maximal frequency of shear wave induced by acoustic radiation force in soft materials (<2 kHz), meaning that we can only focus on the two zero-order modes S_0 and A_0. As is shown in Fig. 1, the axial displacement of the S_0 mode is symmetric, with respect to the median plane of the plate (axial displacement direction does not change when crossing the median plane), whereas the axial displacement of the A_0 mode is antisymmetric (axial displacement direction changes when crossing the median plane). Because the acoustic radiation force pushes in the same direction through the thickness of the plate, it induces mainly antisymmetric mode. Furthermore, the S_0 mode is propagating much faster than the A_0 mode ($v_{S0} \sim 2c_T$), making it harder to detect than the A_0 mode and completely separated from the A_0 mode in the Fourier domain. Finally, in our experimental setup, the A_0 mode is mainly generated and easy to detect as compared with the S_0 mode, which is weakly generated and harder to detect. For a free plate (in vacuum) and for this particular mode, the dispersion equation can be approximated at low frequency, giving an analytical formulation of the phase velocity as a function of the angular frequency ω, the thickness h, and the transverse velocity of the plate c_T (Royer and Dieulesaint 2000):

$$v_{A_0} = \sqrt{\frac{\omega h c_T}{\sqrt{3}}}. \tag{6}$$

For a plate immersed in a nonviscous liquid, the dispersion equation is more complicated and exhibits a damping term that reflects the loss of energy as a result of radiation of the guided wave (then called "leaky Lamb wave") in the surrounding medium (see, *e.g.*, Plona et al. 1976; Vavva et al. 2008):

$$\left(k^2 - k_T^2\right)^2 sin\left(\frac{k_L h}{2}\right) cos\left(\frac{k_T h}{2}\right) + 4k^2 k_T k_L cos\left(\frac{k_L h}{2}\right) sin\left(\frac{k_T h}{2}\right) + i\frac{\rho_0 k_L \omega^4}{\rho k_0 c_T^4} cos\left(\frac{k_T h}{2}\right) cos\left(\frac{k_L h}{2}\right) = 0, \tag{7a}$$

$$k_0^2 + k^2 = \left(\frac{\omega}{c_0}\right)^2 k_T^2 + k^2 = \left(\frac{\omega}{c_T}\right)^2 k_L^2 + k^2 = \left(\frac{\omega}{c_L}\right)^2 k = \frac{\omega}{v}. \tag{7b}$$

In eqn (7a), k is the in-plane wave vector. k_T, k_L and k_0 are defined by the relationships given in eqn (7b), ρ and

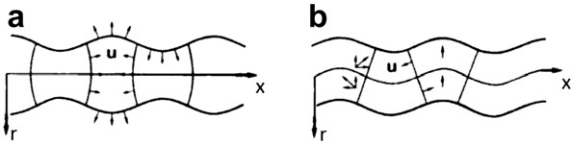

Fig. 1. Illustration of displacements induced by a Lamb wave in a plate: (a) symmetric mode, (b) antisymmetric mode.

ρ_0 are, respectively, the plate and the surrounding fluid density, c_0 is the longitudinal bulk velocity in the fluid and v is the phase velocity.

Impedance contrasts for longitudinal waves are very small in soft tissues (except for fat interface), leading to a very weak reflection coefficient of longitudinal waves. In addition, both theoretical and experimental investigation (see Methods) show that phase velocity is negligible compared with bulk compressional velocity c_L and c_0, which implies $k_0 \approx k_L \approx \sqrt{-k} \approx ik$. According to this assumption, the previous system of equations can be simplified into the following form:

$$\left(k^2-k_T^2\right)^2 sin\left(\frac{ikh}{2}\right)cos\left(\frac{k_T h}{2}\right)+4ik^2k_T k cos\left(\frac{ikh}{2}\right) sin\left(\frac{k_T h}{2}\right)+i\frac{\omega^4}{c_T^4}cos\left(\frac{k_T h}{2}\right)cos\left(\frac{ikh}{2}\right)=0. \quad (8)$$

Unfortunately, the low-frequency expansion of eqn (8) leads to an analytical expression of the phase velocity, which is only valid in the frequency range below 200 Hz for the typical investigated thickness ($h \sim 1$ mm) and bulk shear wave velocity ($c_T \sim 10$ m.s^{-1}) because the low-frequency approximation is valid when: $f << f_m = \frac{c_T}{2\pi h}$. In the investigated range of frequency (>200 Hz), this equation can only be solved numerically. An even more complex situation is the case of a plate embedded in a solid medium. In this case, shear wave leakage is even stronger and the problem with mixed boundary conditions (semi-infinite liquid/solid layer/semi-infinite solid) becomes not tractable analytically. Several numerical methods have been proposed to derive mode propagation in complex medium such as the global matrix method (Lowe 1995). Disperse is a commercial software developed by Lowe et al. that can numerically solve those problems. This software was used in this study to compute numerically the dispersion curves corresponding to the practical investigated situations. These semi-analytical simulations will be considered as our theoretical gold standard. In the Results section, the combination of this exact simulation code with experimental validations will permit us to derive an empirical analytical formula for shear wave dispersion in the arterial wall.

Experimental study: Data acquisition

The ultrasound system used in this study is a modified "Aixplorer" ultrafast scanner developed by the company SuperSonic Imagine (Aix-en-Provence, France). This system is programmable per channel both in receive (128 channels) and in transmit mode (256 channels). It allows switching between the following sequences: conventional B-mode imaging, acoustic radiation force sequence or "push sequence" for the remote generation of shear waves and "ultrafast imaging" sequence to image at very high frame rate the shear wave propagation, as well as natural motion inside the body such as the arterial pulse wave. The ultrasonic probe used in this study (128 elements, 8-MHz central frequency, pitch 0.3 mm, 28-mm elevation focus) was provided by Vermon (Tours, France).

To image the propagation of shear waves, a frame rate above 2000 images/second is required. Plane wave transmit enables the reconstruction of a complete frame from a single transmit/receive event. An entire image is obtained by applying receive-only dynamic beamforming to backscattered echoes, which enables an imaging frame rate equal to the pulse transmit rate (up to 20,000 images/second). To increase both resolution and contrast, coherent compounding of tilted plane waves is used in this study as described by Montaldo et al. (2009). This ultrafast imaging was used to image shear wave propagation. Tissue displacements induced by the acoustic radiation force are in the frequency range of the low kHz. Tissue particle velocities are typically of the order of a few mm/s, whereas the propagation speed of shear wave is typically a few m/s.

The generation of shear wave by acoustic radiation force for SSI imaging is described in detail by Bercoff et al. (2004). Several "pushing beams" are transmitted at three depths, 1-mm spaced and with a mean focal depth centered on the arterial wall to compensate a potential millimetric motion of the arterial wall during the cardiac cycle. The burst length of each pushing beam is 100 μs and induces typically 10-μm wall displacements along the direction of the ultrasonic beam. The positions of these pushing beams are displayed while scanning to help the operator positioning the probe. The acquisition of shear wave propagation was software-triggered when the probe and arterial wall were aligned (Fig. 2).

Experimental study: Postprocessing

For all plane transmit insonifications, radiofrequency ultrasonic backscattered echoes (RF data) are beamformed to obtain a stack of IQ-demodulated complex 2-D images with a demodulation frequency equal to the transmit frequency (from 5 to 11 MHz). A frame-to-frame conventional axial velocity estimation is performed using IQ cross-correlation algorithm. Finally, a "movie" of the axial velocity $V_r(r,x,t)$ is obtained (r = depth, x = line number, t = frame number) at 8000 images/second (a typical example is represented in Fig. 3 for different times). An algorithm based on speckle tracking is also used to automatically track the wall position along the time axis (required for *in vivo* imaging only). The velocity in the arterial wall is then extracted: each line of the image has two intersections with the arterial wall (upper and lower wall) giving rise to two $N \times (T-1)$ matrices, where N is the number of lines (typically

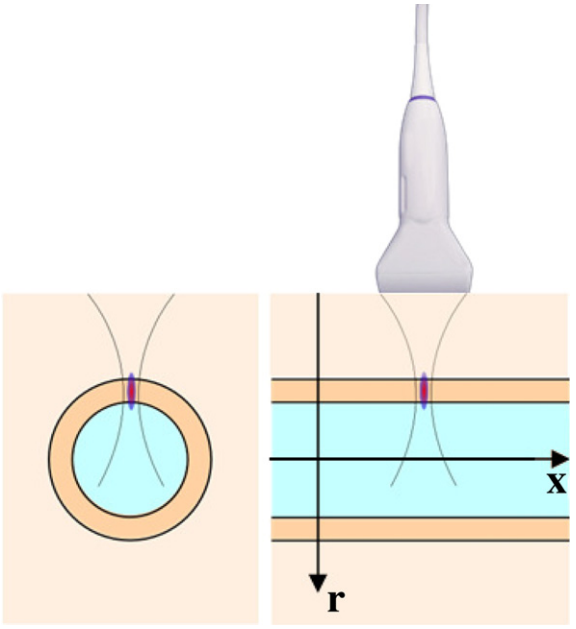

Fig. 2. Experimental setup: The transducer is aligned along the arterial wall. The cylindrical coordinate system (r, z) is represented.

128) and T the number of IQ images (typically 50 images are acquired at a rate of 8000 images/second). The spatio-temporal matrix corresponding to axial particle velocity in the upper wall where shear waves are generated is derived (see Fig. 4b):

$$v_r(x,t) = V_r(r_{wall}(x,t),x,t), \tag{9}$$

where x is the line number (x = 1…N), t is the frame number (t = 1…T−1) and $r_{wall}(x, t)$ the detected position of the upper arterial wall at (x, t).

During a single "push sequence," the acoustic radiation force generates a large band mechanical excitation in the 50−2000 Hz range. Shear waves generated at the focal area are guided by the arterial wall and propagate in a highly dispersive regime (Figs. 3 and 4b). Phase velocity of guided shear wave strongly varies with respect to its spectrum. A direct analysis of the $v_r(x,t)$ matrix is not suitable to extract the dispersion curves because all of the frequencies are mixed in the time domain. First, arterial wall motion caused by the arterial pulse wave (corresponding to large displacements at very low frequency 0 to 20 Hz) is rejected by simply removing the time average of particle velocity on each line of the image. Then, a 2-D Fourier transform (Fig. 5a) is applied on these spatio-temporal filtered data, *i.e.*, motion caused by the shear wave generation corresponding to small displacements at high frequency (∼500 to 2000 Hz) to derive the dispersion curve of each individual mode. The dispersion curves are obtained by finding for each frequency the phase velocity at which the Fourier transform amplitude is maximal, as shown in Fig. 5 (Goldstein and Maugin 2004). These dispersion curves are then used to recover the plate/tube/arterial wall shear modulus: bulk shear wave speed (c_T) is varied in the theoretical curve, corresponding to the considered sample's geometry until it fits the experimental curve (by minimizing the least mean squares). *In vitro*, the geometrical parameters of each sample were known in advance. *In vivo*, thickness and radius of the imaged arterial segments were measured using ultrasound imaging.

In vitro *experiments: Theoretical model validation*

To corroborate theoretical analysis, two experimental situations are investigated *in vitro*: shear wave propagation in soft elastic plates and soft elastic tubes. The propagation of shear waves in thin, soft plates is first investigated to establish a simple propagation model. Then, this model is extended to the propagation along the tube wall, as explained in the Results and Discussion sections. Both tubes and plates are built using the same protocol. A mold of the desired sample was house-machined in a hard material (Plexiglas or steel). Liquid phantom preparations (agar-agar, gelatin or polyvinyl alcohol) are molded in this negative print to obtain samples of a given geometry with various elastic and backscattering properties or samples with the same mechanical properties but different geometries. Three plates of different geometries were made: 1.0-, 1.55- and 2-mm thickness, 4 × 4 cm wide. Tube geometry

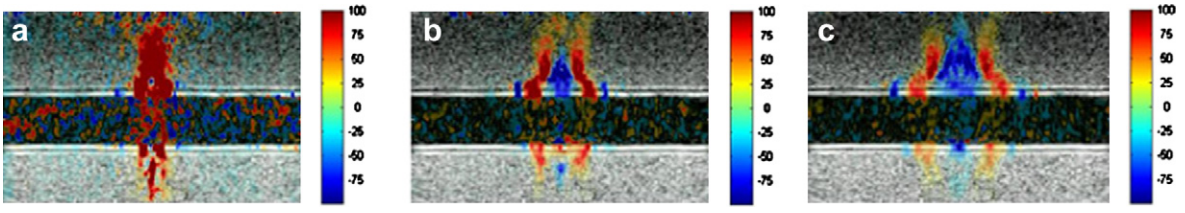

Fig. 3. Shear wave propagation along the superior wall of an arterial phantom (Agar gel) embedded into softer gelatin gel. The axial velocity field (tissue Doppler imaging) is superimposed to the anatomic grayscale image in color (mm/s) at different time steps: t = 0.5 ms (a), t = 2 ms (b) and t = 4 ms (c). The ultrasonic probe is located on the top of the images. The elastic wave propagating along the wall is faster than in the surrounding softer gel.

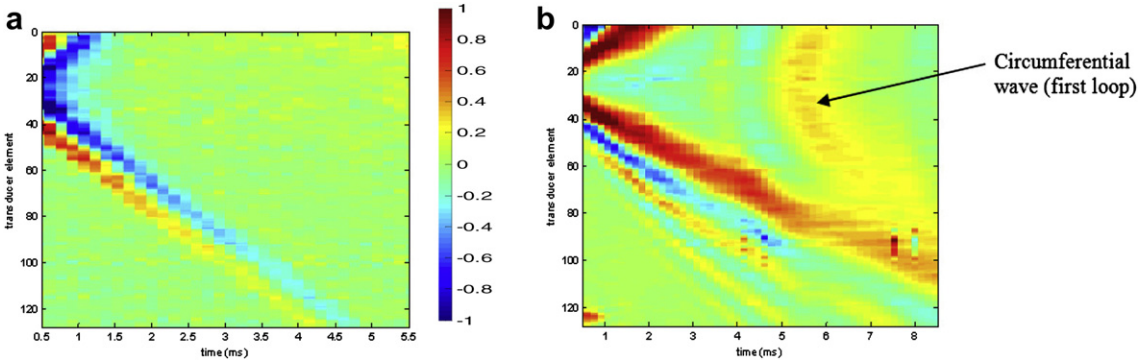

Fig. 4. Normalized space-time representation of tissue particle velocity caused by the shear wave propagation (a) in a homogeneous agar sample and (b) in an Agar tube immersed in water. In (a) and (b), all of the frequency components are originally in phase. In (a), all of the frequency components propagate at the same speed and the pulse shape is not changed. In contrast, in (b), each component propagates at a different speed, which distorts the pulse shape during propagation.

phantoms were made using the same materials. Tube phantoms geometries were 4 mm inner radius; 1-, 1.5- and 2-mm thickness; and 100 mm length.

Plates and tubes are implanted within different soft elastic media. In a first study, phantoms composed of plates or tubes completely immersed in water are investigated. Second, the tubes are filled with water and implanted into a soft gel made of gelatin (4%).

This last phantom is built to mimic arteries filled with blood and surrounded with an outer solid medium.

In vivo *experiments: Real-time shear wave elastography applied to arterial wall elasticity estimation*

Data acquisition and associated postprocessing described in the *in vitro* part were applied *in vivo* on volunteers and on animals. To assess arterial elasticity in real-time during the pulse wave propagation, the sequence of pushes followed by an ultrafast acquisition was repeated 15 times every 70 ms. Therefore, each ultrafast acquisition gives access to an instantaneous elasticity estimation and the whole acquisition covers a complete cardiac cycle during approximately 1 s. Each acquisition was time coregistered with the cardiac cycle owing to an ECG device recording simultaneously the ECG trace of the subject and the ultrasound system trig-out signal at the beginning of each ultrafast acquisition. The acquisition sequence was also gated on the R-wave of the ECG using an ECG device (Accusync 42, Milford, CT, USA) to assess the reproducibility of the technique.

Safety study

All of the elementary acoustic beam patterns (pushing beam, flat beam, focused beam) were characterized before this study for regulatory purpose, allowing to ensure the mechanical index and I_{SPTA} of the specific sequences used in this study to respect Food and Drug Administration recommendations for ultrasound imaging (FDA 2008).

To ensure the safety of the whole procedure, a safety study was performed *in vivo* on large animals (N = 10). This study was conducted with the approval of the Animal Care and Use Committee of the "École de Chirurgie, Assistance Publique-Hôpitaux de Paris." To investigate the safety of the pushing beam on the arterial wall, intensive acquisitions were performed on the left carotid arteries of 10 sheep. For each animal, a series of 15 acquisitions was performed every 70 ms and repeated every 10 s for 1 min. These sonications were performed at the maximum value of transmit voltage (corresponding to 4-MPa peak pressure at focus). The whole experiment was performed at three different sites of the carotid artery. The animal was then sacrificed 48 h after acquisition. The sonicated and nonsonicated carotid artery segments (4 to 5 cm long) were removed, fixed in 10% formalin. After fixation, the artery segments were examined and cut in 0.3-cm-long sections. Eight to 10 segments were embedded in paraffin and analyzed by histology, so that the sampling of tissues allows the analysis of half of the artery segments. Paraffin blocks were cut in 5-μm-thick sections and stained with hematoxylin and eosin and elastic stain for detection of any artery wall disruption, inflammation or necrosis.

In vivo *acquisition*

In vivo feasibility of shear wave imaging was investigated on the 10 sheep before the safety study protocol and also on one 30-year-old healthy volunteer. The human protocol was approved by the "Comité de protection des personnes (CPP) Ile de France" according to French regulations for clinical trials. A conventional B-mode examination was first performed to locate the artery. The common carotid artery was imaged in the longitudinal

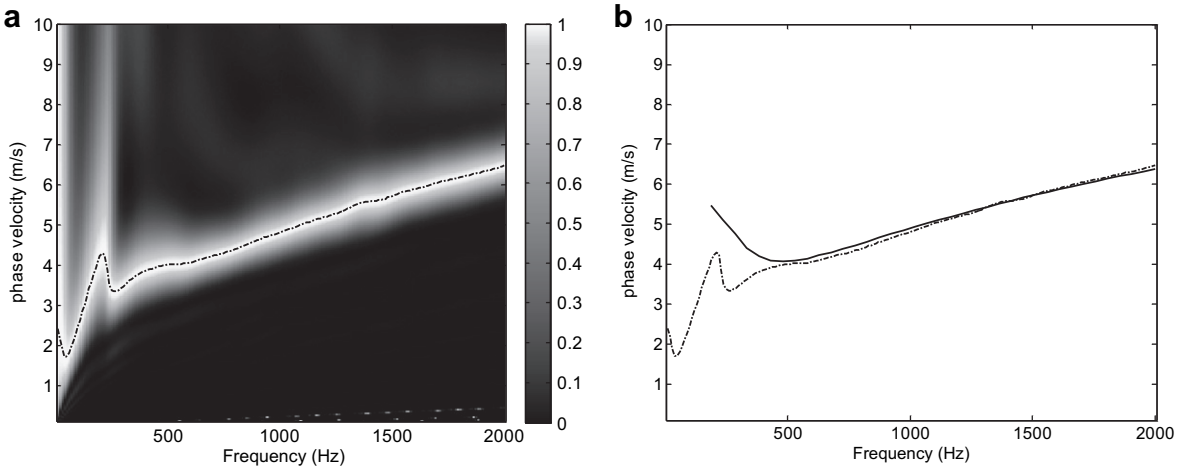

Fig. 5. (a) 2-D Fourier transform (energy) of a spatio-temporal matrix v_r obtained *in vitro*. The energy is normalized to one for each frequency; extracted dispersion curve is also represented (for each frequency, phase velocity at which energy is maximum). (b) Extracted dispersion curve and corresponding theoretical fit.

direction. Ultrafast acquisition of the acoustically induced shear wave propagation in the arterial wall was performed during 20 ms at a frame rate of typically 8000 frame/s. The estimation of the local shear wave speed was then computed from radiofrequency signals as described in the postprocessing section.

RESULTS

In vitro *experiments*

To corroborate theoretical results on shear wave dispersion in the artery with calibrated experiments, remote palpation experiments were performed on plate and tube phantoms. The complete movie of tissue particle velocity as a result of the shear wave propagation was acquired and several frames are shown at different time steps (Fig. 3). One-dimensional speckle tracking performed on B-mode images during the ultrafast acquisition clearly enables imaging the shear wave propagation in the tube wall and in surrounding tissues. In Fig. 3, the mechanical wave propagates much faster in the tube wall than in surrounding tissues. Based on tissue particle velocity estimates inside the wall of arterial phantoms, dispersion curves were computed and compared with the theoretical dispersion of A_0 leaky Lamb waves. In this section, the dispersion was first investigated in plates with different stiffness and thickness immersed in water. Second, the dispersion was investigated in tubes immersed in water. Finally, the study was extended to the case of dispersion in tubes embedded in elastic soft medium to mimic at best the carotid mechanical behavior.

Figure 4 illustrates the importance of the guiding effect of the arterial wall on the shear wave propagation. Figure 4a shows the space-time representation of tissue displacements caused by a shear wave induced by the ultrasonic radiation force in a homogeneous soft tissue-mimicking phantom. Figure 4b shows the same kind of propagation in the constrained space of a soft tube whose thickness is smaller than the shear wavelength. One can clearly notice the strong dispersion occurring in this second experimental configuration. High-frequency components of the wave propagate much faster than low frequency. The shear wave is guided along the tube, mainly in the tube axis direction, but also propagates in the circumferential direction around the tube. The first loop of this circumferential wave is visible in Fig. 4b. The 2-D Fourier transform described in the methods section is applied to each dataset and the corresponding dispersion curves extracted as shown in Fig. 5.

Wave dispersion in a plate embedded in water. The propagation of shear waves in plates with different thickness and stiffness were investigated. A total of four plates of 1- and 1.5-mm in thickness were made using 2% and 4% Agar gels. Figure 6 (a, b) shows that experimental dispersion curves are in good agreement with numerical computation of theoretical dispersion curves when shear modulus was adjusted to 25 kPa for the 2% agar gel and 166 kPa for the 4% agar gel in the numerical model. Shear moduli were also measured on large bulk samples of the material owing to conventional SSI elastography and they were also in good agreement with the previous values as shown in Fig. 7. Moreover, in the case of large bulk sample, the nondispersive behavior of the propagation is obvious because the phase velocity is constant over the frequency spectrum (Fig. 7). As shown in the Methods section, contrary to the case of a free plate (in vacuum), the low-frequency approximation of the dispersion equation (eqn (6)) does not fit both theoretical and experimental dispersion curves in the investigated frequency

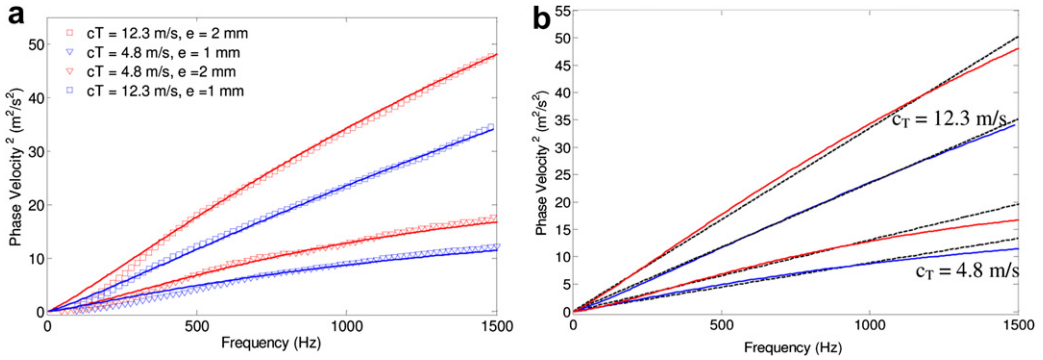

Fig. 6. (a) Experimental dispersion curves for 4% Agar plates (□) and 2% Agar plates (▽) in water. One-mm plates are shown in blue and 1.5-mm plates in red. (c_T = 12.3 m/s for 4% Agar plate, and c_T = 4.8 m/s for 2% Agar plate; c_L was set to 1500 m/s for both plates). (b) Theoretical curves in Fig. 4a are plotted in plain line (—) as well as eqn (10)'s corresponding analytical formula (black, - - -).

range. However, as shown in Fig. 6, the square of the phase velocity was found to be a linear function of the frequency for all the experiments and corresponding numerical simulations based on Lowe semi-analytical implementation. According to this observation, an empirical formula was derived to fit the dispersion curves:

$$V \approx \sqrt{K\frac{\omega h c_T}{\sqrt{3}}} \approx \sqrt{\frac{\omega h c_T}{2\sqrt{3}}}. \qquad (10)$$

Surprisingly, this empirical formula corresponds to the theoretical low-frequency approximation found for the A_0 mode for a plate in vacuum with a numerical correction factor K. By fitting the experimental and simulation curves, the value of K was determined to be equal to 0.5 ± 0.07. The fitting provided by the empirical formula was compared with both the numerical simulations and the experimental results in Fig. 6 (a, b). The empirical formula provided in eqn (10) nicely describes the propagation of shear wave in soft plates embedded in water. The following subsection investigates its applicability in the case of tubes embedded in water or soft solids.

Wave dispersion in a tube embedded in water. To investigate the influence of the tube geometry on the propagation of the shear wave, similar experiments were performed in cylindrical shells immersed in water. Cylindrical shells were made using the same material than the plate, with an inner diameter of 8-mm and a wall thickness of 1 mm. Figure 7 shows the experimental and numerical dispersion curves for a plate and a tube of the same thickness. Although the phase velocity differs from the plate in the low-frequency range, the two dispersion curves converge toward the same values when frequency increases. Indeed, for low frequencies, the shear wavelength becomes comparable with the diameter of the tube, which induces a strong influence of the tube geometry. However, for higher frequencies, this influence becomes smaller and Fig. 7 shows that the empirical formula (eqn (10)) becomes a good approximation above 1000 Hz. Therefore, the shear modulus of an immersed tube can be estimated using the high-frequency part of the curve (>1000 Hz) based on the model developed for a plate and applying eqn (10) as a theoretical fitting curve. Furthermore, one can notice that in certain cases, even if the theoretical curve fits the experimental one at high frequency, a strong discrepancy can be observed at low frequency between the two curves because that

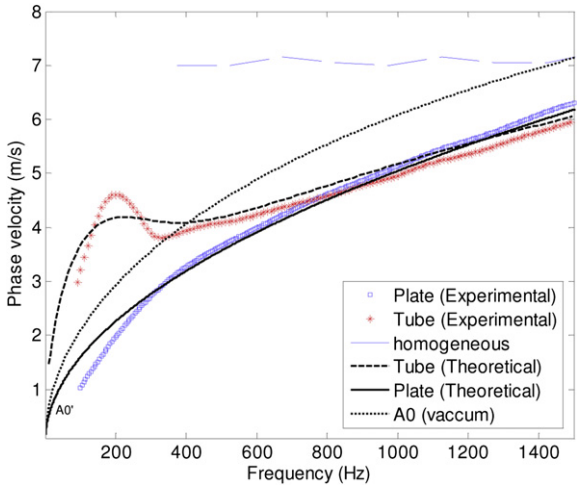

Fig. 7. Experimental dispersion curves of a shear wave propagation in the same solid medium for different geometrical configurations: bulk homogeneous sample (.), 1-mm agar plate (□) and (*) cylindrical shell immersed in water. Theoretical curves (semi-analytical approach, Lowe 1995) are shown in black for the plate mode in vacuum (A0) (…), in water (A0′) (-) and for the cylindrical shell mode (- -). The shear velocity was set to 12.3 m/s and bulk velocity to 1500 m/s.

wavelength becomes as large as the scanning area at low frequency. This is why the theoretical *fit is performed only on the high-frequency part of the curve (>500 Hz).*

These results are confirmed for two tubes of different stiffness used in this study (Fig. 8): the empirical formula found for plate in water can also provide an estimate of the shear modulus for a tube in water.

Wave dispersion in a tube embedded in a solid medium and filled with water. The influence of the outer medium was investigated numerically by embedding the tubes in a soft elastic medium of varying stiffness. Numerical dispersion curves were obtained and compared with the case of tube immersed in water. Typical values for geometric and elastic properties of the carotid artery (inner diameter 4 mm, thickness 1 mm and shear wave speed c_T = 12 m/s) were used, whereas the Young's modulus of the surrounding medium was varied from 0–532 kPa (corresponding to a shear wave speed ranging from 0–12 m/s). Figure 9 shows that the curves do not vary significantly when the surrounding medium remains softer than 48 kPa. In vivo, tissue elasticity remains almost always softer than this value. However, if the outer medium becomes stiffer, dispersion could be affected, requiring the use of this complete propagation model to estimate correctly the arterial wall shear modulus.

Shear wave in vivo *experiments*

Safety study. In the proposed method, the limiting transmit pattern for the mechanical index is the pushing beam, whose maximal value was below 0.6 for each transmitted beam. The total I_{SPTA} for the sequence applied *in vivo* was 630 mW/cm^2. In all tissue samples, gross examination did not show any abnormalities (Fig. 10).

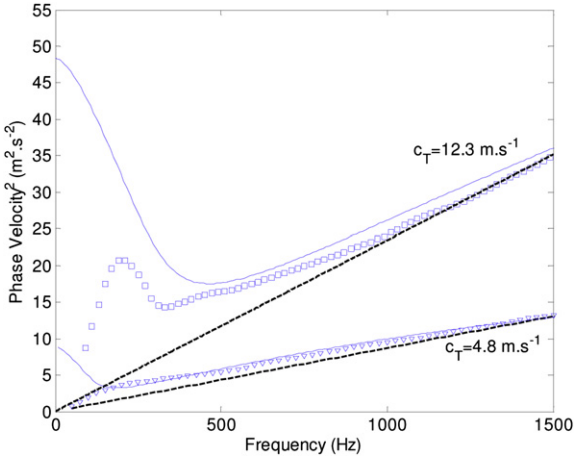

Fig. 8. Experimental dispersion curve for 1-mm cylindrical shells made of 4% Agar (□) and 2% Agar (▽). The theoretical curve (*black*) is shown for each phantom (-) as well as the analytical formula eqn (10) (- -) using the parameters used in Fig. 4.

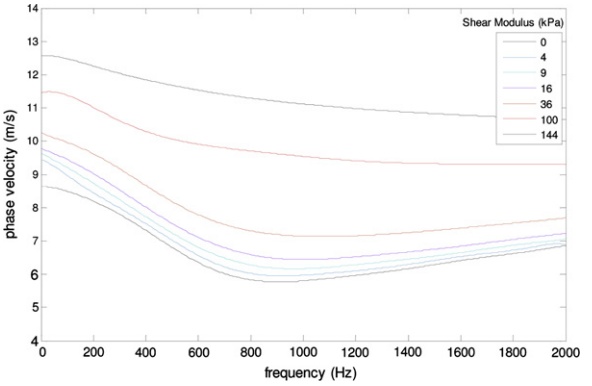

Fig. 9. Influence of surrounding medium: numerical computation of dispersion curves obtained for a tube of 4-mm inner diameter and 1-mm thickness, c_T = 12 m/s, filled with water and various case of surrounding medium: μ = 0, 4, 9, 16, 36, 100, 144 kPa.

At histology, the artery wall was constantly normal, ruling out any vascular wall cell damage and inflammation.

Real-time shear wave elastography applied to arterial wall elasticity estimation. The right common carotid artery of a volunteer was scanned using real-time shear wave elastography, allowing elasticity estimation of the carotid artery 10 times within one cardiac cycle. Figure 11 shows successive snapshots of the shear wave propagation in the arterial wall. Similar to results in phantoms, the shear wave velocity was found to be approximately three times higher in the arterial wall than in surrounding tissues. The dispersion analysis was performed on the *in vivo* data up to 1500 Hz. It clearly demonstrates the ability of ultrasonic radiation force to generate very-high-frequency shear waves *in vivo*.

The shape of *in vivo* shear wave dispersion is very close to *in vitro* curves and it was possible to estimate the shear modulus by measuring the wall thickness (h = 0.95 mm) and the artery radius (R = 2.90 mm) on the echo image and fitting the experimental curve with a theoretical curve obtained using the Disperse software. As shown on Fig. 12, a good fit is obtained with both the theoretical curve and the empirical formula. One should notice that the empirical formula (eqn (10)) does not require the knowledge of the artery radius *R* because it corresponds to a high-frequency approximation where the wavelength is smaller than the radius.

The elasticity of the arterial wall was found to be time-dependent during one cardiac cycle (Table 1, Fig. 13). These values are in the range of healthy arterial stiffness measured using other techniques (O'Rourke et al. 2002). As a result of the simultaneous acquisition of both ECG signal and trigger out of the ultrasound system, it was possible to correlate the elasticity variation with the different stages of the heart cycle. Figure 13a

Fig. 10. Histological cut of sonicated (*right*) and nonsonicated artery (*left*).

presents the 15 successive space-time distributions of tissue particle velocity in the arterial wall acquired within a single cardiac cycle. One clearly notices on each successive set of data the presence of a propagating wave generated by the radiation force generation. This wave radiates from the middle of the image (line 64) and propagates transversally in both directions. Moreover, strong and different motion offsets are present in the successive ultrafast acquisitions (see the change in color baseline at each successive acquisition in Fig. 13a). These offsets correspond to the additional motion of the arterial wall as a result of the arterial pulse during the ultrafast acquisition. Because the arterial pulse contains very low frequencies (<20 Hz), wavelengths associated pulse wave are much larger than wavelengths shear waves induced by radiation. Arterial pulse wavelengths are even larger than the imaging area width (>5 cm), resulting in a spatially homogeneous offset in each ultrafast acquisition. During the systolic event, induced shear wave is superimposed on the natural pulse wave. Figure 13b corresponds to the same dataset after filtering of this homogeneous offset for each ultrafast acquisition. One can clearly notice that this filtering enables discriminating both waves. Using the radiation force–induced wave, the arterial stiffness was found to increase rapidly during systolic event and decrease slowly during diastolic event, as shown in Fig. 13c. Finally, the *in vivo* reproducibility of the measurement was assessed on the volunteer using 10 independent acquisitions. The standard deviation of the phase velocity was 0.2 m/s at 1200 Hz and the standard deviation of the shear-derived shear modulus was 8 kPa at early systole and 12 kPa at end systole.

The same acquisition sequence was performed on 10 sheep. The shear phase velocity and dispersion curves were derived between 100 and 1500 Hz, and the minimum shear modulus was found in early systole (R peak), whereas the maximum shear modulus was found in end systole (T wave). These results are summarized in Table 1.

DISCUSSION

In this paper, we have proposed a new technique for the estimation of the arterial stiffness: a broadband, guided shear wave (100 to 1500 Hz) is generated in the arterial wall using the ultrasonic radiation force and imaged at high frame rate to derive the arterial wall stiffness. The model proposed in the Methods section has been validated *in vitro* and the feasibility of the technique was shown *in vivo*. Moreover, the shear wave can be generated several times per second and thus enables the estimation of elasticity variation during the cardiac cycle. However, the dispersion of this wave (shown to be a leaky

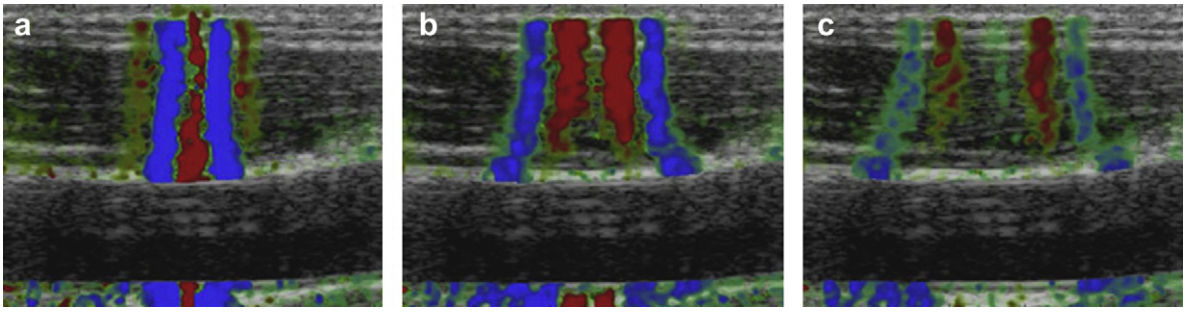

Fig. 11. *In vivo* experiment in the carotid artery: propagation of shear wave generated by acoustic remote palpation and acquired by ultrafast imaging: Color-coded axial displacements are superimposed to grayscale anatomic B-mode and represented at t = 0.5 ms (a), t = 2 ms (b) and t = 4 ms (c) after the generation of the acoustic radiation force.

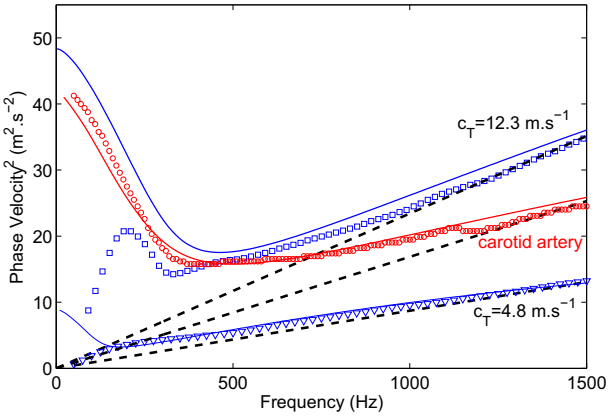

Fig. 12. Experimental dispersion curves obtained in arterial phantoms with different shear modulus (*blue square*) compared with numerical solutions (*solid blue line*); *in vivo* in the common carotid arterial wall of a healthy volunteer (*red square curve*) compared with numerical simulation (*solid red line curve*).

A_0 Lamb wave) is complex and has been carefully studied here. In this paper, a very simple model was tested *in vitro* to investigate the propagation of shear wave in soft layers ($c_T << c_L$) immersed in water. We demonstrated experimentally the suitability of this model to explain shear wave dispersion in soft agar plates immersed in water (c_L = 1.54 mm/s, c_T <12 m/s, with thickness of 1.0, 1.5 mm). In this case, the dispersion equation can be solved numerically and this semi-analytical solution can be used to fit the experimental dispersion curve in a wider range of frequencies, shear modulus and thicknesses to retrieve the elastic modulus that is supposed to be unknown.

Another even simpler approach was also proposed in this paper as a formula derived empirically from *in vitro* experimental data (eqn (10)), which can also give a rough estimation of shear modulus from experimental dispersion curves. In the case of a tube immersed in water, which is closer to the case of the arterial wall, a plate model is still valid to estimate shear wave modulus by considering only the highest frequencies (>1 kHz) to fit experimental dispersion curves. When a tube is filled with water and surrounded by a softer medium, a plate model can again be used as an approximation to fit experimental data. This equation was shown to give a very good approximation of the shear wave dispersion. It permits to recover Young's modulus from the knowledge of the mechanical wave speed and the arterial wall thickness. Nevertheless, in the extreme case of a small contrast in shear modulus between arterial wall and surrounding medium, this formulation will not correctly describe the situation and the complete dispersion relation of the system needs to be solved numerically, taking into account the shear modulus of the surrounding medium. The average shear modulus of the surrounding medium can be estimated easily using conventional shear wave elastography mode (Bercoff et al. 2004; Tanter et al. 2008). Then this value would be used in this numerical model to fit experimental dispersion curves.

Another parameter to be determined for numerical dispersion curves computation to fit experimental one is the thickness and eventually the radius of the tube (in the extreme cases where the empirical formula is not valid anymore). The intima-media thickness is commonly measured using ultrasound imaging because it is a well-accepted indicator for pathologies such as atherosclerosis or diabetes. However, the different arterial layers (intima, media, adventitia) have different elasticity (Fung 1993). According to our simple model, we only consider an average elasticity of effective arterial layers.

Finally, the ability to follow in real time the arterial wall elasticity was demonstrated in this paper. A single ultrafast acquisition of the shear wave propagation in the arterial wall was performed in less than 10 ms and allowed the estimation of the arterial stiffness. Although traveling together, both mechanical waves (arterial pulse and radiation force–induced wave) can be separated by straightforward signal processing. To our knowledge, it is the first time that elasticity of the arterial wall was measured noninvasively, quantitatively and instantaneously at different periods of the cardiac cycle. This opens the possibility of measuring not only the arterial elasticity but also its variation over the cardiac cycle caused by cardiac pulsatility. In this study, the shear modulus was measured up to 15 times during a cardiac cycle, but higher acquisition rate could be achieved by repeating acquisitions every 10 ms, which would correspond to as many as 85 elasticity measurements over one cardiac cycle.

Because viscoelastic properties of the arterial wall vary with the arterial pressure over the cardiac cycle, it is important to measure the elastic modulus at a precise timing of the cardiac cycle. On the other hand, the

Table 1. *In vivo* results

			Blood pressure (mm Hg)		Carotid dimensions (mm)		Shear modulus (kPa)	
	N	Heart rate (bpm)	Systole	Diastole	Diameter	Thickness	Early-systole	End-systole
Human	1	60	112	63	5.8	0.95	86	134
Sheep	10	103 ± 10	96 ± 9	67 ± 5	5.45 ± 0.51	1.2 ± 0.1	117 ± 48	173 ± 77

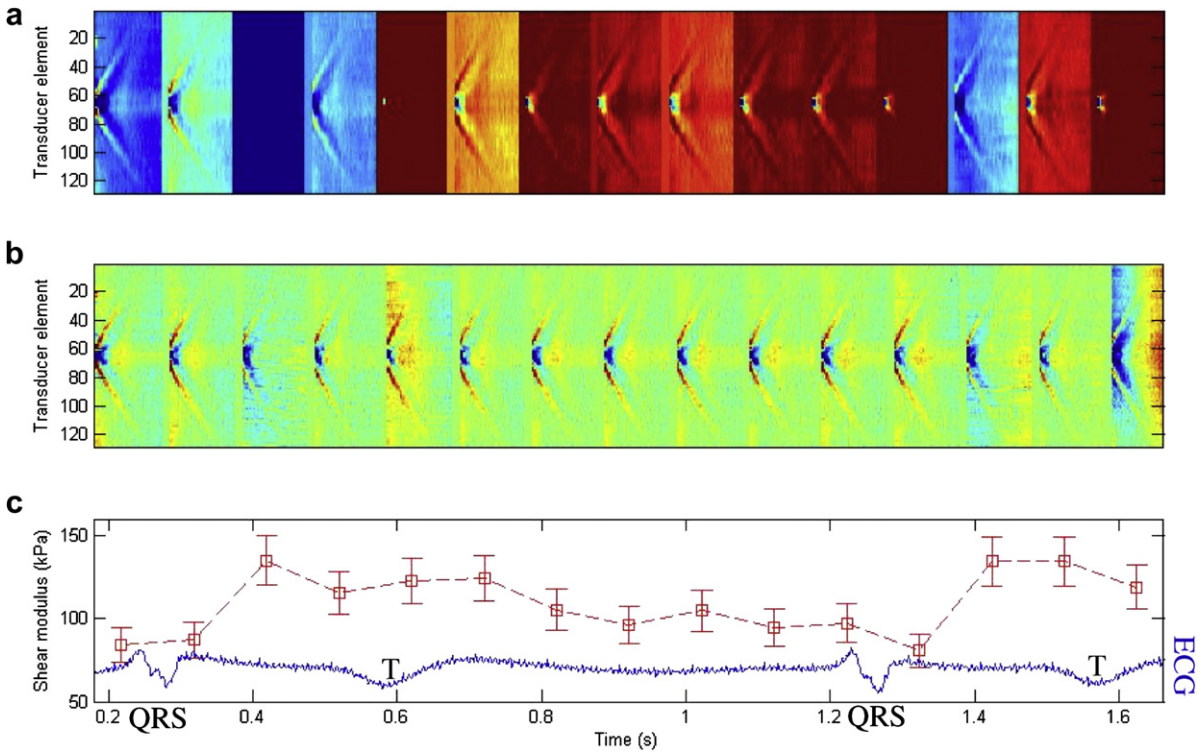

Fig. 13. Real-time *in vivo* measurement of carotid arterial wall shear modulus variation during a single heart cycle (13 values/cycle) with time-registered ECG. (a) 15 successive space-time representations of tissue particle velocity in the arterial wall. One clearly notices on each successive set of data the presence of a propagating wave caused by the radiation force generation. (b) The same dataset after filtering of the homogeneous velocity offset as a result of the arterial pulse wave propagation for each ultrafast acquisition. One can clearly notice that this filtering enables discriminating both waves (arterial pulse wave and radiation force–induced wave). (c) Shear modulus deduced from each ultrafast acquisition owing to the estimation of the wave speed of the radiation force–induced wave.

nonlinearity of elasticity could be an important parameter to measure for clinical diagnosis. Nonlinearity of elasticity has been measured invasively *in vivo* on arteries (Barra et al. 1993): stress/strain curves were obtained for a large range of intravascular pressure. In our study, the variation of the shear modulus was observed on a single cardiac cycle. Consequently, the investigated pressure range was smaller. The shear modulus of the carotid wall was measured to be 130 kPa ± 15 kPa in systole and 80 kPa ± 10 kPa in diastole. These results show that a strong variation of the elastic properties occurs during the cardiac cycle, which means that the nonlinear coefficient of elasticity of the carotid arterial wall is high. A precise evaluation of the nonlinearity of the arterial wall would require measuring the arterial pressure over the cardiac cycle. With our setup, the variation of the shear modulus of the arterial wall under transmural stress can be written as (Catheline et al. 2003; Landau and Lifshitz 1959):

$$\mu = \mu_0 + \frac{A}{12\mu_0}\sigma, \tag{11}$$

where μ_0 is the shear modulus at zero stress, A the nonlinear elastic coefficient (known as the Landau coefficient) and σ the local uni-axial stress. Based on this equation, the nonlinear elastic coefficient can be expressed as a function of the diastolic and systolic pressure and shear modulus:

$$A = 12\mu_0 \frac{\mu_{syst} - \mu_{diast}}{P_{syst} - P_{diast}} \sim 12\mu_{diast} \frac{\mu_{syst} - \mu_{diast}}{P_{syst} - P_{diast}}, \tag{12}$$

where μ_{syst} and μ_{diast} are, respectively, the systolic and diastolic shear modulus and P_{syst} and P_{diast} are, respectively, the systolic and diastolic arterial pressure at the considered site.

A difference of 30 mm Hg is usually found between systolic and diastolic pressure in healthy subjects, but it can increase significantly with pathologies such as hypertension. For the investigation on one volunteer, it gives a typical A = 11.1 kPa for the Landau coefficient describing arterial wall elastic nonlinearity.

In this paper, shear wave propagation was investigated along the longitudinal direction of the arterial wall. To derive the shear modulus, we assumed that the

viscoelastic properties of the arterial wall were isotropic and for the sake of simplicity, the arterial wall was assumed to be purely elastic. This assumption is also done in the Moens-Korteweg equation, which is well accepted to derive the wall elasticity from the pulse wave velocity. However, several studies have shown that the arterial wall exhibits a different shear modulus in the longitudinal and circumferential directions (Fung 1993). Although most of the existing techniques including PWV and echo tracking provide an estimate of the circumferential Young's modulus, the SSI technique gives access to the longitudinal shear modulus because shear wave propagation is analyzed in the longitudinal direction. The measurements of both circumferential and longitudinal shear moduli using conventional arterial stiffness techniques combined with shear wave imaging could potentially be of great importance for the prediction and diagnosis of cardiovascular diseases.

CONCLUSION

In this paper, the dynamic behavior of arterial wall biomechanical properties during the cardiac cycle has been exhibited. The novelty of the present work lies in the *in vivo* applicability of quantitative and real-time elasticity assessment using the acoustic radiation force. The ultrafast acquisition was used to image shear wave propagation in the arterial wall induced by acoustic radiation force. Shear wave propagation was found to be very dispersive as a consequence of both arterial geometric and elastic properties (thin, hard layer filled with liquid and embedded in a softer medium). This dispersion effect has to be considered to retrieve the elastic shear modulus μ. An analytical formula was derived to retrieve this modulus from the dispersion curve obtained experimentally. The feasibility of measuring the arterial stiffness using this technique has been demonstrated both *in vitro* in an arterial model and *in vivo* in the common carotid artery of one volunteer. A variation of the shear modulus over the cardiac cycle was found *in vivo* ($80 < \mu < 130$ kPa). The high potential of this technique for clinical assessment of arterial stiffness is demonstrated, because this technique is fully quantitative, noninvasive and can be performed in real time (10 times per second).

Acknowledgments—This work was supported by a grant from the ANR TECSAN (France).

SUPPLEMENTARY DATA

Supplementary data associated with this article can be found, in the online version, at doi:10.1016/j.ultrasmedbio.2010.07.004.

REFERENCES

Ambartsumyan SA, Movsisyan LA. Propagation of a pulse wave. Mech Composite Mat 1978;14:569–573.

Asmar R, Benetos A, Topouchian J, Laurent P, Pannier B, Brisac A, Target R, Levy BI. Assessment of arterial distensibility by automatic pulse wave velocity measurement: Validation and clinical application studies. Hypertension 1995;26:485–490.

Barra J, Armentano R, Levenson J, Fischer E, Pichel R, Simon A. Assessment of smooth muscle contribution to descending thoracic aortic elastic mechanics in conscious dogs. Circ Res 1993;73: 1040–1050.

Bercoff J, Pernot M, Tanter M, Fink M. Monitoring thermally-induced lesions with supersonic shear imaging. Ultrason Imaging 2004a; 26:71–84.

Bercoff J, Tanter M, Fink M. Supersonic shear imaging: A new technique for soft tissue elasticity mapping. IEEE Trans Ultrason Ferroelectr Freq Control 2004b;51:396–409.

van den Berkmortel FW, van der Steen M, Hoogenboom H, Wollersheim H, van Langen H, Thien T. Progressive arterial wall stiffening in patients with increasing diastolic blood pressure. J Hum Hypertension 2001;15:685–691.

Bolster BD Jr, Atalar E, Hardy CJ, McVeigh ER. Accuracy of arterial pulse-wave velocity measurement using MR. J Magn Reson Imaging 1998;8:878.

Boutouyrie P, Laurent S, Benetos A, Girerd XJ, Hoeks AP, Safar ME. Opposing effects of ageing on distal and proximal large arteries in hypertensives. J Hypertension Suppl 1992;10:S87–S91.

Bramwell JC, Hill AV. The velocity of the pulse wave in man. Proceedings of the Royal Society of London. Series B. Containing Papers of a Biological Character 1922;93:298–306.

Catheline S, Gennisson JL, Fink M. Measurement of elastic nonlinearity of soft solid with transient elastography. J Acoust Soc Am 2003;114: 3087.

Cheng K, Baker CR, Hamilton G, Hoeks APG, Seifalian AM. Arterial elastic properties and cardiovascular risk/event. Eur J Vasc Endovasc Surg 2002;24:383–397.

Deffieux T, Montaldo G, Tanter M, Fink M. Shear wave spectroscopy for in vivo quantification of human soft tissues visco-elasticity. IEEE Trans Med Imaging 2009;28:313–322.

Deng SX, Tomioka J, Debes JC, Fung YC. New experiments on shear modulus of elasticity of arteries. Am J Physiol Heart Circ Physiol 1994;266:H1–H10.

Eriksson A, Greiff E, Loupas T, Persson M, Pesque P. Arterial pulse wave velocity with tissue Doppler imaging. Ultrasound Med Biol 2002;28:571–580.

Fung YC. Biomechanics—Mechanical properties of living tissues. New York: Springer; 1993.

Goldstein RV, Maugin GA. Surface waves in anisotropic and laminated bodies and defects detection. New York: Springer; 2004.

Hasegawa H, Kanai H. Simultaneous imaging of artery-wall strain and blood flow by high frame rate acquisition of RF signals. IEEE Ultrason Ferroelectr Freq Control 2008;55:2626–2639.

Hermeling E, Reesink KD, Kornmann LM, Reneman RS, Hoeks AP. The dicrotic notch as alternative time-reference point to measure local pulse wave velocity in the carotid artery by means of ultrasonography. J Hypertension 2009;27:2028–2035.

Kanai H, Umezawa A, Koiwa Y. Transcutaneous measurement of frequency dispersion in the regional pulse wave velocity. IEEE Ultrason Symp 2000.

Korteweg D. Ueber die Fortpflanzungsgeschwindigkeit des Schalles in elastischen Röhren 1878;525.

Landau LD, Lifshitz EM. Theory of Elasticity. New York: Pergamon Press; 1986.

Laurent S, Boutouyrie P, Asmar R, Gautier I, Laloux B, Guize L, Ducimetiere P, Benetos A. Aortic stiffness is an independent predictor of all-cause and cardiovascular mortality in hypertensive patients. Hypertension 2001;37:1236–1241.

Laurent S, Cockcroft J, Van Bortel L, Boutouyrie P, Giannattasio C, Hayoz D, Pannier B, Vlachopoulos C, Wilkinson I, Struijker-Boudier H. Expert consensus document on arterial stiffness: Methodological issues and clinical applications. Eur Heart J 2006;27: 2588.

Lowe MJS. Matrix techniques for modeling ultrasonic waves in multilayered media. IEEE Trans Ultrason Ferroelectr Freq Control 1995;42:525–542.

Mahieu D, Kips J, Rietzschel ER, De Buyzere ML, Verbeke F, Gillebert TC, De Backer GG, De Bacquer D, Verdonck P, Van Bortel LM, Segers P. Noninvasive assessment of central and peripheral arterial pressure (waveforms): Implications of calibration methods. Journal of Hypertension 2010;28:300–305.

Meinders JM, Hoeks AP. Assessment of local pulse wave velocity in arteries using 2D distension waveforms. Ultrasound Med Biol 2003;29:S57.

Mersich B, Rigó J, Besenyei C, Lénárd Z, Studinger P, Kollai M. Opposite changes in carotid versus aortic stiffness during healthy human pregnancy. Clin Sci (London 1979) 2005;109:103–107.

Montaldo G, Tanter M, Bercoff J, Benech N, Fink M. Coherent plane-wave compounding for very high frame rate ultrasonography and transient elastography. IEEE Trans Ultrason Ferroelectr Freq Control 2009;56:489–506.

Muller M, Gennisson JL, Deffieux T, Tanter M, Fink M. Quantitative viscoelasticity mapping of human liver using supersonic shear imaging: Preliminary in vivo feasibility study. Ultrasound Med Biol 2009;35:219–229.

O'Rourke MF, Staessen JA, Vlachopoulos C, Duprez D, Plante GE. Clinical applications of arterial stiffness; definitions and reference values. Am J Hypertension 2002;15:426–444.

Paini A, Boutouyrie P, Calvet D, Zidi M, Agabiti-Rosei E, Laurent S. Multiaxial mechanical characteristics of carotid plaque: Analysis by multiarray echotracking system. Stroke 2007;38:117.

Pernot M, Fujikura K, Fung-Kee-Fung SD, Konofagou EE. ECG-gated, mechanical and electromechanical wave imaging of cardiovascular tissues in vivo. Ultrasound Med Biol 2007;33:1075–1085.

Plona TJ, Pitts LE, Mayer WG. Ultrasonic bounded beam reflection and transmission effects at a liquid/solid-plate/liquid interface. J Acoust Soc Am 1976;59:1324–1328.

Royer D, Dieulesaint E. Elastic waves in solids, vol. 1. Berlin, Heidelberg: Springer-Verlag; 2000.

Sarvazyan AP, Rudenko OV, Swanson SD, Fowlkes JB, Emelianov SY. Shear wave elasticity imaging: A new ultrasonic technology of medical diagnostics. Ultrasound Med Biol 1998;24:1419–1435.

Schaar JA, de Korte CL, Mastik F, Strijder C, Pasterkamp G, Boersma E, Serruys PW, van der Steen AF. Characterizing vulnerable plaque features with intravascular elastography. Circulation 2003;108: 2636–2641.

Shadwick RE. Mechanical design in arteries. J Exp Biol 1999;202:3305.

Sorensen GL, Jensen JB, Udesen J, Holfort IK, Jensen JA. Pulse wave velocity in the carotid artery. IEEE Ultrason Symp 2008.

Tanter M, Touboul D, Gennisson J, Bercoff J, Fink M. High-resolution quantitative imaging of cornea elasticity using supersonic shear imaging. IEEE Trans Med Imaging 2009;28:1881–1893.

Tanter M, Bercoff J, Athanasiou A, Deffieux T, Gennisson J, Montaldo G, Muller M, Tardivon A, Fink M. Quantitative assessment of breast lesion viscoelasticity: Initial clinical results using supersonic shear imaging. Ultrasound Med Biol 2008;34:1373–1386.

Trahey GE, Palmeri ML, Bentley RC, Nightingale KR. Acoustic radiation force impulse imaging of the mechanical properties of arteries: In vivo and ex vivo results. Ultrasound Med Biol 2004; 30:1163–1171.

Vavva MG, Protopappas VC, Gergidis LN, Charalambopoulos A, Fotiadis DI, Polyzos D. The effect of boundary conditions on guided wave propagation in two-dimensional models of healing bone. Ultrasonics 2008;48:598–606.

Xiaoming Zhang, Kinnick R, Fatemi M, Greenleaf J. Noninvasive method for estimation of complex elastic modulus of arterial vessels. IEEE Trans Ultrason Ferroelectr Freq Control 2005;52: 642–652.

Zhang X, Greenleaf JF. Estimation of complex arterial elastic modulus from ring resonance excited by ultrasound radiation force. Ultrasonics 2006;44:e169–e172.